Solution Structure of the Ternary Complex between Aminoacyl-tRNA, Elongation Factor Tu, and Guanosine Triphosphate †

ARTICLE *in* BIOCHEMISTRY · JULY 1998

Impact Factor: 3.02 · DOI: 10.1021/bi9802869 · Source: PubMed

Solution Structure of the Ternary Complex between Aminoacyl-tRNA, Elongation Factor Tu, and Guanosine Triphosphate†

N. Bilgin,*,‡ M. Ehrenberg,‡ C. Ebel,§ G. Zaccai,§,|| Z. Sayers,⊥ M. H. J. Koch,⊥ D. I. Svergun,⊥,▽ C. Barberato,⊥,○ V. Volkov,⊥,▽ P. Nissen,# and J. Nyborg#

Department of Molecular Biology, The Biomedical Center, Uppsala University, Box 590, S-751 24 Uppsala, Sweden, Institut de Biologie Structurale, 41 Avenue des Martyrs, F-38027 Grenoble Cedex 1, France, European Molecular Biology Laboratory, EMBL c/o DESY, Notkestrasse 85, D-22603 Hamburg, Germany, Institute of Crystallography, Russian Academy of Sciences, Leninsky pr.59, 117333, Moscow, Russia, Department of Molecular and Structural Biology, Aarhus University, Gustav Wieds Vej 10c, DK-8000 Aarhus C, Denmark, and Institut Max Von Laue−Paul Langevin, Avenue des Martyrs, B.P. 156, F-38042 Grenoble Cedex 9, France

Received February 4, 1998; Revised Manuscript Received March 23, 1998

ABSTRACT: Complex formation between elongation factor Tu (EF-Tu), Phe-tRNA^{Phe}, and GTP was analyzed by small-angle neutron and X-ray scattering methods. Both techniques show that the ternary complex consists of one EF-Tu and one aminoacyl-tRNA. No shift in stoichiometry was detected when the temperature was raised from 5 to 37 °C, in contrast to previous observations obtained from RNase A protection experiments [Bilgin and Ehrenberg (1995) *Biochemistry 34*, 715−719]. A small but significant increase in the radius of gyration of the complex was observed when the temperature was decreased from 37 to 5 °C. The X-ray solution scattering patterns were compared with those calculated from the crystal structure of the complex formed between EF-Tu from *Thermus aquaticus* and Phe-tRNA^{Phe} from yeast. The comparison shows that the solution structure of the ternary complex, formed entirely from *Escherichia coli* components and under translationally optimal buffer conditions, is very close to the crystal structure, formed from heterologous components under very different conditions. Furthermore, for the hybrid complex in solution there is no evidence for the formation of trimers as suggested by the crystal structure.

Elongation factor Tu (EF-Tu) is a prokaryotic G-protein that binds every aminoacylated elongator tRNA in a ternary complex with GTP and brings it to the A-site of the mRNA-programmed ribosome (*1*). When the anticodon of the incoming aminoacyl-tRNA matches the A-site codon, GTP on EF-Tu is rapidly hydrolyzed (*2*, *3*) and EF-Tu•GDP leaves the ribosome, allowing transfer of the nascent polypeptide from the donor peptidyl-tRNA in the P-site to the acceptor aminoacyl-tRNA in the A-site (*1*). Binding of cognate aminoacyl-tRNAs to the A-site of programmed ribosomes is 4 orders of magnitude faster when they are in complex with EF-Tu and GTP, compared to when they bind nonenzymatically (Helen Pahverk and Måns Ehrenberg, unpublished results). The accuracy of aminoacyl-tRNA selection is enhanced by EF-Tu and GTP by more than 1 order of magnitude (Helen Pahverk and Måns Ehrenberg, unpublished results). Dissociation of GDP from EF-Tu is accelerated by elongation factor Ts by about 3 orders of magnitude (*4*), making regeneration of the ternary complex from EF-Tu•GDP adequately fast.

In contrast to these previous results, Ehrenberg et al. (*5*) presented experiments, showing that two GTPs are hydrolyzed per peptide bond on EF-Tu in poly(U) translation by ternary complexes that contain Phe-tRNA^{Phe}. They also analyzed the stoichiometry of the ternary complex with biochemical methods, developed by Tapio et al. (*6*), and found that 2 molecules of EF-Tu seemed to be required to protect 1 Phe-tRNA^{Phe} molecule from spontaneous deacylation. To explain these data, Ehrenberg et al. (*5*) suggested that the ternary complex is "extended" and contains 2 EF-Tu•GTP complexes bound to 1 aminoacyl-tRNA.

The interaction between *Escherichia coli* EF-Tu, GTP, and Valyl-tRNA^{Val} has been studied by Antonsson et al. (*7*) by using small-angle neutron scattering. These authors performed titrations of the protein by increasing aminoacyl-tRNA concentrations up to a molar ratio of 2, so that conditions corresponding to a large excess of tRNA over protein were not examined. Their data were consistent with a monomer−dimer equilibrium for free EF-Tu. Upon addition of aminoacyl-tRNA, however, the dimers dissociated

† This work was supported by grants from The Swedish Natural Science Research Council (to M.E. and N.B.), NATO Linkage Grant LG921231, INTAS Grant 93-645 (to M.H.J.K.), INTAS Grants 95-1272 and 96-1115 (to M.H.J.K., D.I.S., and V.V.), EMBO short-term fellowship (to N.B.), Conselho Nacional de Desenvolvimento Cientifico e Technologico (Brasil) predoctoral fellowship (to C.B.), and Biotechnology Program of The Danish Research Council (to P.N. and J.N.).

* Corresponding author. Present address: Department of Biochemistry, The Biomedical Center, Uppsala University, Box 576, S-751 23 Uppsala, Sweden. Tel +46 18 4714987; fax +46 18 511755; e-mail bilgin@xray.bmc.uu.se.

‡ Uppsala University.

§ Institut de Biologie Structurale.

|| Institut Max Von Laue−Paul Langevin.

⊥ EMBL.

▽ Russian Academy of Sciences.

○ Present address: Laboratorio Nacional de Luz Sincrotron, C. P. 6192, 13081−870, Campinas, SP, Brasil.

Aarhus University.

S0006-2960(98)00286-4 CCC: $15.00
Published on Web 06/02/1998

into monomers in favor of 1:1 complex formation so that they found a stoichiometry of 1 EF-Tu/1 aminoacyl-tRNA for the ternary complex. Dimers (about 15%) were also present in samples of halophilic EF-Tu from *Haloarcula marismortui* obtained from standard purification procedures but their interaction with aminoacyl-tRNA has not been studied (*8*). The notion of an extended ternary complex was criticized by Bensch et al. (*9*), who used 4 different types of experiments to show that there is only 1 molecule of EF-Tu bound to 1 aminoacyl-tRNA.

Weijland and Parmeggiani (*10*) and Weijland et al. (*11*) presented experiments apparently confirming the finding by Ehrenberg et al. (*5*) that 2 GTPs are hydrolyzed on EF-Tu for every peptide bond in poly(U) translation.

In contrast, Rodnina and Wintermeyer (*12*) reported experiments on ribosomes initiated on heteropolymeric mRNAs containing a Shine and Dalgarno sequence and an initiation codon (AUG) followed by different in-frame codons. They found that in most of their codon contexts there is only 1 GTP hydrolyzed on EF-Tu/peptide bond, but for the mRNA sequence AUG·UUU·UUC they observed 2 GTPs hydrolyzed on EF-Tu when the last Phe codon UUC was translated by Phe-tRNA^{Phe}. From this result they suggested, first, that an extra GTP is hydrolyzed in EF-Tu function in slippery codon contexts, where there is high probability for a frameshift error. Second, they rationalized this finding by hypothesizing that hydrolysis of an extra GTP molecule is required to prevent frameshifts. They also presented evidence from gel-filtration experiments for the existence of an extended ternary complex when there is EF-Tu in excess over aminacyl-tRNA.

The stoichiometry of the ternary complex was further analyzed by Bilgin and Ehrenberg (*13*) at different temperatures using RNase A protection experiments in combination with quench-flow techniques. These biochemical results suggested that only 1 EF-Tu is required to protect 1 aminoacyl-tRNA at low temperatures, but 2 molecules of EF-Tu are required to protect 1 aminoacyl-tRNA from RNase A cleavage at high temperatures, again supporting the notion of an extended ternary complex at 37 °C.

The crystal structure of the ternary complex (*14*) contains 1 aminoacyl-tRNA bound to 1 molecule of EF-Tu and 1 GTP analogue. Furthermore, in these crystals, the asymmetric unit consists of 3 ternary complexes forming a trimer intercorrelated by a 3-fold axis. It was speculated that the trimer plays a physiological role. This ternary complex structure is composed of EF-Tu from *Thermus aquaticus* and aminoacyl-tRNA from yeast and it was crystallized under conditions very different from those under which the biochemical stoichiometry experiments described above were performed. One possibility was therefore that the 1:1 stoichiometry in the crystal structure was caused by special conditions. It was, furthermore, conceivable that the 2:1 stoichiometry obtained with biochemical methods under more optimal conditions for protein synthesis reflected the physiologically relevant composition of the ternary complex. These contradictory results have caused a confusing situation and the present work aims at clarifying what the stoichiometry of the ternary complex really is under different conditions and whether it can be brought to change. The approach was to analyze the structure of the ternary complex under precisely those conditions where the biochemical data reporting 2:1 stoichiometry had been obtained and where protein synthesis is known to work optimally in vitro (*5*, *6*, *13*).

The data obtained here with small-angle neutron and X-ray scattering techniques demonstrate that there is a 1:1 stoichiometry between EF-Tu and aminoacyl-tRNA under all conditions used and that the crystal and solution structures of the ternary complex are remarkably similar.

MATERIALS AND METHODS

Purification of E. coli EF-Tu. EF-Tu was isolated from frozen *E. coli* MRE 600 cells, harvested during logarithmic growth, and purified according to Ehrenberg et al. (*15*). Purified factor was extensively dialyzed against polymix buffer (*16*) in the presence of 10 mM GDP [polymix buffer contains: 5 mM magnesium acetate, 0.5 mM calcium chloride, 95 mM potassium chloride, 5 mM ammonium chloride, 8 mM putrescine, 1 mM spermidine, 5 mM potassium phosphate (pH 7.3), and 1 mM 1,4-dithioerythritol (DTE)]. EF-Tu was homogeneous as judged by SDS−PAGE. The protein content of the purified EF-Tu was determined by amino acid analysis of the protein hydrolyzate and by colorimetric assay of the intact protein (*17*). The active EF-Tu concentration was determined by nitrocellulose filter assay for GDP binding to EF-Tu and by nucleotide exchange assay for conversion of GDP to GTP on EF-Tu as a function of time as described by Ehrenberg et al. (*15*). These four independent concentration measurements were in full agreement for the EF-Tu preparation used in the present work.

Purification of Phe-tRNA Synthetase. Phe-tRNA synthetase (PRS) was purified as a side product from the EF-Tu preparation as described by Ehrenberg et al. (*15*) with further modifications: During EF-Tu preparation, fractions with PRS activity were pooled from the DEAE-cellulose (CL-6B, Pharmacia). After ammonium sulfate fractionation between 38% and 50%, PRS was further purified by gel-filtration chromatography on AcA 44 (IBF) followed directly by ion-exchange chromatography on FPLC using Q-Sepharose (FF) (Pharmacia). PRS was dialyzed against polymix buffer containing 50% glycerol and was stored at −20 °C. PRS was homogeneous as judged by SDS−PAGE.

Purification of E. coli tRNA^{Phe}. tRNA^{Phe} was purified from frozen *E. coli* MRE 600 cells. All purification steps were carried out at room temperature. tRNA$_{bulk}$ was prepared by phenol extraction of the cells followed by 1 M NaCl fractionation, and DEAE-cellulose (DE-52, Whatman) chromatography. tRNA^{Phe} was purified from tRNA$_{bulk}$ by benzoylated-DEAE-cellulose (Boehringer) chromatography (*18*). Final purification was achieved by reverse-phase chromatography on Sepharose 4B (Pharmacia) (*19*) at 4 °C. tRNA^{Phe} was extensively dialyzed against polymix buffer and stored at −20 °C. This preparation of tRNA^{Phe} was aminoacylatable to 1394 pmol of Phe-tRNA^{Phe}/OD$_{260}$.

Preparation of [^{14}C]Phe-tRNA^{Phe}. tRNA^{Phe} (500 nmol) was preparatively aminoacylated in the presence of 1500 nmol of [^{14}C]Phe (specific activity of 3.7 cpm/pmol), 5500 units of PRS (1 unit aminoacylates 1 pmol of tRNA/s), 1 mM ATP (Pharmacia), 10 mM PEP (Sigma), 250 μg of pyruvate kinase (EC 2.7.1.40, Boehringer), and 15 μg of myokinase (EC 2.7.4.3, Sigma) in 7.5 mL of reaction volume

in polymix buffer. Aminoacylation was for 15 min at 37 °C. Two volumes of ethanol were added to stop the reaction and precipitate the aminoacyl-tRNA. After the precipitate was collected by centrifugation, Phe-tRNA^{Phe} was further purified at 4 °C on a benzoylated-DEAE-cellulose column (20 mL) and aminoacyl-tRNA was eluted with 1.4 M NaCl containing 20% ethanol. After precipitation with two volumes of ethanol and collection of the tRNA by centrifugation, Phe-tRNA^{Phe} was dialyzed extensively against polymix buffer. For those neutron scattering experiments that were performed in 70% D_2O, a fraction of the Phe-tRNA^{Phe} was dialyzed against polymix buffer prepared in 89.5% D_2O (Sigma, 99.9%, see below). Phe-tRNA^{Phe} prepared this way had a final aminoacylation of 1545 pmol of Phe-tRNA^{Phe}/OD_{260} in polymix and 1684 pmol of Phe-tRNA^{Phe}/OD_{260} in polymix with 89.5% D_2O.

Complex Formation between EF-Tu·GTP and Phe- tRNA^{Phe} from E. coli: Phe-tRNA^{Phe} Titrations in H_2O or in 70% D_2O. Each sample was prepared for a 150 μL final reaction volume balanced in polymix buffer containing 1 mM ATP, 10 mM PEP, 1 mM GTP, 5 μg of pyruvate kinase, 0.3 μg of myokinase, 112 units of PRS and 30 nmol of [^{14}C]Phe (3.7 cpm/pmol) with or without 120 μM EF-Tu. To achieve identical conditions between samples, all components except the tRNA were prepared in a 32.7 μL volume for each sample. To this mixture was added 117.3 μL of Phe-tRNA^{Phe} to give final concentrations between 0 and 240 μM in two series (one in ordinary polymix, the other in polymix with 89.5% D_2O). The final D_2O concentration in all samples of the latter series was 70%. The ternary complex was allowed to form for 15 min at 37 °C, after which the samples were kept on ice until the measurement.

EF-Tu Titrations at a Fixed tRNA Concentration. Three series were prepared, each in 150 μL of final reaction volume, as described above but lacking Phe. The first series was in the absence of tRNA, the second contained 100 μM Phe-tRNA^{Phe}, and the third contained 100 μM (deacylated) tRNA^{Phe}. The EF-Tu concentrations were 0, 100, and 200 μM for the series without tRNA or with deacylated tRNA^{Phe}. For the samples containing Phe-tRNA^{Phe}, the EF-Tu concentrations were between 0 and 333 μM. The ternary complex was allowed to form for 15 min at 37 °C. Samples were then kept on ice until the measurement.

Preparation of the Ternary Complex between Yeast Phe-tRNA^{Phe} and T. aquaticus EF-Tu·GDPNP for Solution Scattering Experiments. The yeast Phe-tRNA and *T. aquaticus* EF-Tu·GDPNP ternary complex, identical to the crystallized and structurally described complex, was prepared as described by Nissen et al. (*20*). The sample for small-angle neutron scattering experiments contained 1.8 mg/mL complex (26 μM) in 30 mM Tris-HCl (pH 7.6), 7.5 mM 2-(*N*-morpholino)ethanesulfonic acid (MES), 1.82 M ammonium sulfate, 10 mM $MgCl_2$, 0.5 mM NaN_3, 0.5 mM dithiothreitol (DTT), and 0.2 mM GDPNP (final pH 6.8). Thus, the solvent in this sample closely resembled the mother liquor during crystal growth.

Small-Angle Neutron Scattering (SANS) Measurements. SANS measurements were performed on the D11 camera (*21*, *22*) at the Institut Laue Langevin (Grenoble, France). The momentum transfer range and resolution were adapted to the molecular dimensions examined by varying the sample to detector distance ($S-D$) and the neutron wavelength λ. Conditions were chosen with $S-D = 2.8$ m, $\lambda = 1.0$ nm, and a momentum transfer range of $0.15 \leq s \leq 0.8$ nm^{-1} [$s = 4\pi \sin(\theta)/\lambda$]. 2θ is the scattering angle. (Note that $s = Q$, the term that is conventionally used in SANS measurements. This unified definition for scattering vector is used throughout the text.) Samples were in quartz cuvettes of 0.100 cm path length (sample volume of about 150 μL), placed in an automatic sample changer whose temperature was controlled by a thermostated water bath. Exposures were quantified by a low-efficiency monitor in the incident beam.

Isotropic scattering data from the 64 × 64 cm^2 pixel detector were radially averaged and stored as neutron counts per pixel as a function of s for a given monitor count [$I(s)$]. They were put on an absolute scale by calibration against the $I(s)$ of 0.100 cm of H_2O measured under identical conditions described by Jacrot and Zaccai (*23*). After subtraction of buffer scattering, the $I(s)$ from a dilute, monodisperse macromolecular solution can be interpreted using the Guinier approximation (*24*):

$$\ln I(s) = \ln I(0) - {}^1/_3 R_g{}^2 s^2 \qquad (1)$$

Fitting a straight line to $\ln I(s)$ versus s^2 determines the parameters $I(0)$ and $R_g{}^2$, where R_g is the radius of gyration of contrast amplitude in the macromolecule. The molecular weight of the macromolecular particle can be calculated from $I(0)$ and the sample concentration, c (*23*). The Guinier approximation is strictly valid only for dilute solutions in which interparticle effects can be neglected. However, these effects may occur even in dilute solutions, e.g., for charged macromolecules in low ionic strength solution. Therefore a concentration series should be measured to obtain values of $I(0)$ and $R_g{}^2$ from extrapolations to $c = 0$. When, as in the present case, the sample contains a mixture of macromolecules (e.g., EF-Tu and tRNA), $I(0)$ and $R_g{}^2$ correspond to weighted averages and can be interpreted in terms of component values (*25*).

Small-Angle Solution X-ray Scattering (SAXS). Data were collected on the X33 camera (*26*) of the European Molecular Biology Laboratory (EMBL) in HASYLAB on the storage ring DORIS of the Deutsches Elektronen Synchrotron (DESY) in Hamburg. Scattering patterns at 5 and 37 °C were recorded using a standard data acquisition system (*27*, *28*) with a multiwire proportional detector (*29*) covering the range of momentum transfer $0.125 \leq s \leq 1.95$ nm^{-1}. Data were collected in 10 time frames of 1 min each, and comparison of the scattering data from different frames indicated no radiation damage. Data in successive frames were normalized to the intensity of the direct beam, corrected for detector response, and averaged, and scattering from the buffer was subtracted. The statistical errors were propagated throughout this process using the program SAPOKO (Svergun and Koch, unpublished results). Distance distributions, radii of gyration (R_g), and forward scattering [$I(0)$] were evaluated using the indirect transform package GNOM (*30*, *31*).

Evaluation of Solution Scattering Patterns. The atomic models were taken from the Brookhaven Protein Data Bank, entries 1EFT for the EF-Tu (*32*), 4TRA for the tRNA (*33*), and 1TTT for their complex (*14*). The scattering amplitudes and the solution scattering curves from the models of the

EF-Tu and the tRNA were calculated using the program CRYSOL (*34*) as

$$I(s) = \langle |A(\boldsymbol{s})|^2 \rangle_\Omega = \langle |A_a(\boldsymbol{s}) - \rho_s A_s(\boldsymbol{s}) + \delta\rho_b A_b(\boldsymbol{s})|^2 \rangle_\Omega \quad (2)$$

Here $\boldsymbol{s} = (s, \Omega)$ is the scattering vector [note that $s = Q = 4\pi \sin(\theta)/\lambda$ here], $A_a(\boldsymbol{s})$ is the scattering amplitude of the particle in vacuo, $A_s(\boldsymbol{s})$ and $A_b(\boldsymbol{s})$ are, respectively, the scattering amplitudes of the excluded volume and the solvation shell, and $\langle\ \rangle_\Omega$ stands for the average over all particle orientations. The solvation shell is represented by a hydration layer of 0.3 nm thickness with an adjustable density ρ_b, which may differ from that of the bulk solvent ρ_s, and $\delta\rho_b = \rho_b - \rho_s$. The spherical average in eq 2 is facilitated by the use of the spherical harmonics expansion over all non-hydrogen atoms; those having covalently bound hydrogens in the polypeptide chain are replaced by the atomic groups with corresponding scattering form factors. To properly calculate the scattering from the hydrogens in the tRNA model, a version of CRYSOL has been written generating the atomic groups in the polynucleotide chain. The program varies two parameters, the excluded volume of the particle and the contrast of the hydration layer $\delta\rho_b$, to minimize the discrepancy between the experimental $[I_{exp}(s_j)]$ and calculated $[I(s_j)]$ curves:

$$x^2 = \frac{1}{N-1} \sum_{j=1}^{N} \left[\frac{I(s_j) - I_{exp}(s_j)}{\sigma(s_j)} \right]^2 \quad (3)$$

where $\sigma(s_j)$ is the standard deviation on $I_{exp}(s_j)$ and N is the number of the experimental points.

The scattering intensity, $I(s)$, from the EF-Tu·tRNA complex was evaluated from the scattering amplitudes of both components computed by CRYSOL as

$$I(s) = I_{EfTu}(s) + I_{tRNA}(s) + 2\,\langle A_{EfTu}(\boldsymbol{s})\, A^*_{tRNA}(\boldsymbol{s}, \boldsymbol{u}) \rangle_\Omega \quad (4)$$

where $\boldsymbol{u}$ is the vector between the centers of mass of the EF-Tu and tRNA in the complex. The amplitudes of a shifted particle required for the calculation of the cross-term were obtained by using the multipole expansion method as described by Svergun (*35*, *36*).

Singular Value Decomposition of the X-ray Scattering Data Matrix of the Titration Experiments. The scattering of a multicomponent system is a linear combination of the scattering from each of its K components. It is, in principle, possible to estimate the individual contribution from each of the K scattering components to the total scattering by applying factor analysis to the data set (*37*). However, such estimates assume a normal distribution of errors and are in practice unreliable due to systematic errors. Therefore, two semiempirical methods (*38*, *39*) were used. These methods rely on singular value decomposition of the $M \times P$ data matrix **D**, which has M columns corresponding to the scattering patterns sampled at P values of the scattering vector:

$$\mathbf{D} = \mathbf{U}\cdot\mathbf{W}\cdot\mathbf{V}^{\mathrm{T}} \quad (5)$$

The columns of the rectangular $P \times M$ matrix **U** are the vectors of the matrix $\mathbf{D}\cdot\mathbf{D}^{\mathrm{T}}$, **V** is an $M \times M$ matrix consisting of the eigenvectors of the matrix $\mathbf{D}^T\cdot\mathbf{D}$, **W** is the diagonal matrix of the singular values w_i, with i running from 1 to M, which are the nonnegative square roots of the eigenvalues of $\mathbf{D}\cdot\mathbf{D}^{\mathrm{T}}$ or $\mathbf{D}^T\cdot\mathbf{D}$ arranged in descending order. Assuming that $K < M < P$ and that there is no noise in the original data, then the number of nonzero singular values of the data matrix **D** (i.e. the rank of **D**) is equal to K.

With noisy data, however, **D** has the full rank M. The number of nonnoise components can then be estimated from a plot of the magnitudes of the logarithms of the singular values against their ordinal numbers as described by Guller et al. (*38*). The ordinal number of the rightmost singular value in the high slope region of such a plot (see Figure 7) gives the number of components. This method is useful as long as the noise level does not exceed about 3% and it was the case. A second estimate of K was based on an analysis of the fluctuations in a plot of the columns of the singular matrix **U** against the scattering vector (see Figure 7). Singular vectors, where noise dominates, are characterized by rapid fluctuations and are usually associated with small singular values. Singular vectors arising from the actual components are, in contrast, normally smooth. The number, U, of singular vectors representing such smooth behavior can be established using a nonparametric criterion for randomness of fluctuations in vector data (*40*). This estimate depends on the choice of significance level and may therefore be subjective if there are systematic errors. In the case of scattering data, which are sampled at an interval much smaller than that corresponding to the inverse of the maximum distance (D_{max}) in the particles, the shapes of the singular vectors provide a more objective estimate. In the present case, the two estimates clearly indicated that the number K of components was three ($K = 3$). Therefore, the relative amounts of the different species in solution, spanning the matrix **C** below, were known and the component scattering curves could be found by least-squares analysis from the following overdetermined ($M > K$) system of linear equations:

$$\mathbf{C}\cdot\mathbf{Y} = \mathbf{D} \quad (6)$$

where **C** is an $M \times K$ matrix and Y is the $K \times P$ row matrix of the scattering of each of the K components. The condition number cond(C) of the matrix **C**

$$\mathrm{cond}(C) = w_{max}/w_{min} \quad (7)$$

where w_{max} and w_{min} are the largest and smallest singular values in the diagonal matrix **W** in eq 5 can be interpreted as an upper limit of the magnification of the relative error in the norm of the solution compared to the norm of the relative error in the input data as described by Lawson and Hanson (*41*), either in matrix **C** or in matrix **D**. A small value of cond(C) guarantees a high stability of the numerical solution. To solve eq 6 the singular value decomposition of the concentration matrix was first computed as

$$\mathbf{C} = \mathbf{U}\cdot\mathbf{W}\cdot\mathbf{V}^{\mathrm{T}} \quad (8)$$

and the resultant matrix of individual scattering curves of the components **Y** was obtained as

$$\mathbf{Y} = \mathbf{V}\cdot\mathbf{W}^{-1}\cdot\mathbf{U}^{\mathrm{T}}\cdot\mathbf{D} \quad (9)$$

The value of the residual R in the least-squares process was computed as an average over the partial residuals

$$r_i = \frac{1}{P}\sum_{k=1}^{P}\left| d_{ik} - \sum_{j=1}^{k} c_{ij} y_{jk} \right| \qquad (10)$$

The sample number is i, d_{ik} is the experimental value of the scattering in channel k for sample i, c_{ij} is the concentration of the jth component for sample i, and y_{jk} is the calculated scattering from component j in channel k.

A series of solutions of eq 6 was calculated and the final solution was obtained by eliminating the two curves that had the largest partial residuals and therefore were considered to arise from mixing errors or background subtraction errors.

Since the errors in the matrix **C** in eq 8 were large, it was not possible to estimate reliably the propagation of errors in the scattering data. However, the small values of cond(C) (between 8.5 and 13) suggest that the obtained solutions are stable against experimental errors.

Nondenaturing PAGE. EF-Tu·GTP·Phe-tRNA^{Phe} complex formation was analyzed by nondenaturing polyacrylamide gel electrophoresis. The samples before and after the neutron and X-ray scattering experiments were mixed with 0.1 volume of 50 % glycerol (containing traces of bromphenol blue) and applied to 5% polyacrylamide gels (19:1). PAGE was for 3 h at 4 °C (40 mA, 100 V) with a circulating electrophoresis buffer (10 mM MES, 10 mM magnesium acetate, 65 mM ammonium acetate, 1 mM Na-EDTA, 1 mM DTE, and 10 μM GTP at pH 6.7). Protein bands were visualized by staining with Coomassie brilliant blue.

Phe-tRNA^{Phe}·EF-Tu·GDPNP Crystal Structure. The ternary complex of yeast Phe-tRNA^{Phe}, *T. aquaticus* EF-Tu, and a nonhydrolyzable GTP analogue, GDPNP, was crystallized at a concentration of approximately 10 mg/mL (140 μM) in 1.95 M ammonium sulfate, 10 mM $MgCl_2$, 30 mM Tris-HCl (pH 7.7), 7.5 mM MES, 0.5 mM DTT, 0.5 mM NaN_3, and 0.7 mM GDPNP (final pH 6.8) at 4 °C by vapor diffusion (*20*). The crystal structure was solved at 0.27 nm resolution using X-ray diffraction data collected at 100 K on a shock-frozen crystal (*14*). The structure (PDB entry 1TTT) consisting of three ternary complexes in the asymmetric unit (14 523 non-hydrogen atoms) was refined applying noncrystallographic symmetry restraints and restrained individual temperature factors, which led to a final R-factor of 21.7% and an R_{free} of 29.2% for the 2.50−0.27 nm data (80 769 reflections total, 96% complete, 5% excluded for R_{free}). The solvent structure (approximately 65% of the crystal) was not thoroughly investigated.

The structure revealed an elongated shape of the ternary complex with a rather small interface between EF-Tu·GDPNP and Phe-tRNA, located at the T-loop face of the tRNA acceptor helix and at the nucleotide binding face of EF-Tu·GDPNP (Figure 10). The D-arm and the anticodon arm extend from the complex. The overall dimensions are 11.5 nm by 6.4 nm by 4.0 nm. Almost all interactions between EF-Tu and Phe-tRNA revealed from the crystal structure represent highly conserved features of both macromolecules with respect to sequence or structure.

RESULTS

Small-angle neutron and X-ray solution scattering were used to determine the molar mass of the ternary complex between EF-Tu, GTP, and aminoacyl-tRNA. Either EF-Tu·GTP or Phe-tRNA^{Phe} was titrated, while the other ligand was kept constant to establish that at one point along the titration curve all components were in complex and none free. At this very point in a titration the molar mass of the complex can be precisely estimated. Such titrations also reveal whether the stoichiometry of the complex shifts, as one moves from a situation with excess aminoacyl-tRNA to one with excess EF-Tu·GTP. Precise experiments require that all EF-Tu is active in aminoacyl-tRNA binding and that most tRNA is aminoacylated and competent in EF-Tu binding.

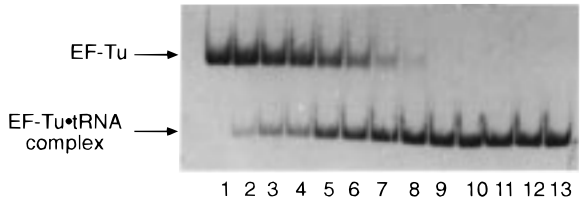

FIGURE 1: Nondenaturing PAGE analysis for the activity of EF-Tu used in the scattering experiments for tRNA binding. EF-Tu was kept at 10 μM and Phe-tRNA^{Phe} was varied (from left to right: 0, 0.9, 1.7, 2.3, 3.7, 4.6, 5.9, 6.7, 7.9, 8.7, 9.6, 12, and 15 μM, respectively). Complex formation and PAGE was as described in Materials and Methods.

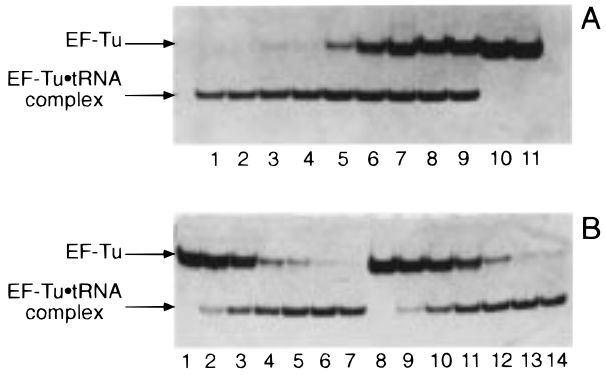

FIGURE 2: Nondenaturing PAGE analysis for ternary complex formation for the samples after SANS measurements. (A) Samples from EF-Tu titration: with 100 μM Phe-tRNA^{Phe} (lanes 1−9), without tRNA (lane 10), or with 100 μM tRNA^{Phe} (lane 11). EF-Tu was present at 53, 67, 80, 100, 133, 167, 200, 267, and 333 μM, respectively (lanes 1−9) and at 200 μM (lanes 10 and 11). (B) Samples from tRNA titration: EF-Tu was present at 120 μM in all samples in polymix buffer (lanes 1−7) or in polymix buffer containing 70% D_2O (lanes 8−14). Phe-tRNA was at 0, 25, 53, 76, 107, 168, and 231 μM (lanes 1−7) and at 0, 22, 47, 69, 93, 138, and 194 μM (lanes 8−14), respectively.

Nondenaturing PAGE Reveals That All EF-Tu Is Competent in Aminoacyl-tRNA Binding. The activity of EF-Tu in forming a complex with Phe-tRNA^{Phe} was studied by nondenaturing PAGE. Phe-tRNA^{Phe} was titrated from 0 to 20 μM with EF-Tu·GTP constant at 10 μM, and aliquots were applied to the gel (Figure 1). The upper band with free EF-Tu·GTP disappears completely and all EF-Tu is recovered in the lower band at sufficiently high concentrations of aminoacyl-tRNA, showing that all EF-Tu is active in ternary complex formation. The activity of EF-Tu in ternary complex formation during scattering experiments was tested by taking aliquots from the samples before and after both the neutron and X-ray experiments. EF-Tu remained active throughout all incubations and measurements under the beam (see Figure 2 for neutron scattering).

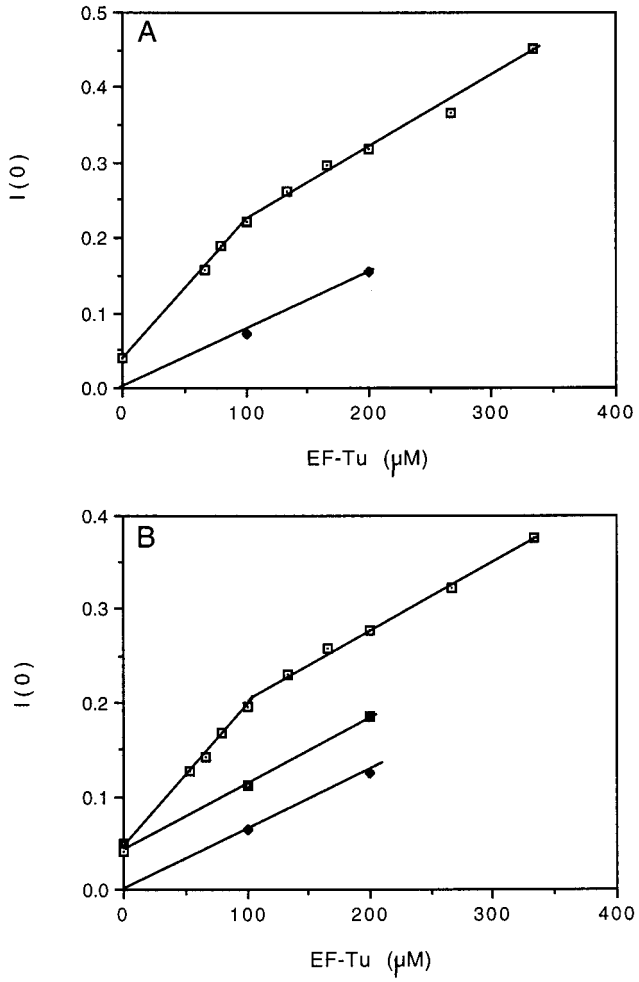

FIGURE 3: (A) SANS measurements at 6 °C at constant concentration of Phe-tRNA^{Phe} (100 μM) with varying EF-Tu concentration. $I(0)$ is plotted as a function of EF-Tu in the absence of tRNA (◆) or with 100 μM Phe-tRNA^{Phe} (⊡). (B) As in panel A but at 37 °C. $I(0)$ is plotted as a function of EF-Tu in the absence of tRNA (◆), with 100 μM of tRNA^{Phe} (◘), and with 100 μM Phe-tRNA^{Phe} (⊡).

Neutron Scattering: (A) E. coli EF-Tu·GTP·Phe-tRNA^{Phe} Complex. Extrapolation from Guinier plots (*24*) gave estimates for the neutron forward scattering at zero angle, $I(0)$, at different concentrations of EF-Tu, and for different EF-Tu·tRNA mixtures (Figure 3). These data were normalized to an absolute scale (*23*) and interpreted in terms of free protein, free tRNA, and complex by using their concentrations, their calculated neutron scattering amplitudes, and solvent scattering density, as described in detail by Dessen et al. (*42*).

The lowest two sets of points in each panel of Figure 3 illustrate how $I(0)$ depends on EF-Tu concentration in the absence of tRNA, at 6 and 37 °C, respectively. The data points fit reasonably well with the lines calculated for the known molar mass of EF-Tu (43 150 g/mol) at 6 and 37 °C, respectively (*23*). The slope corresponding to the correct molar mass indicates that there is no aggregation of EF-Tu molecules at either temperature, despite the large concentrations used in these experiments. On the other hand, the points lying slightly below the line are consistent with either an interparticle effect or an overestimate of EF-Tu concentration. The corresponding radii of gyration (R_g) were constant at 2.5 nm, however, making the existence of interparticle effects unlikely, in these conditions. At 37 °C, the filled

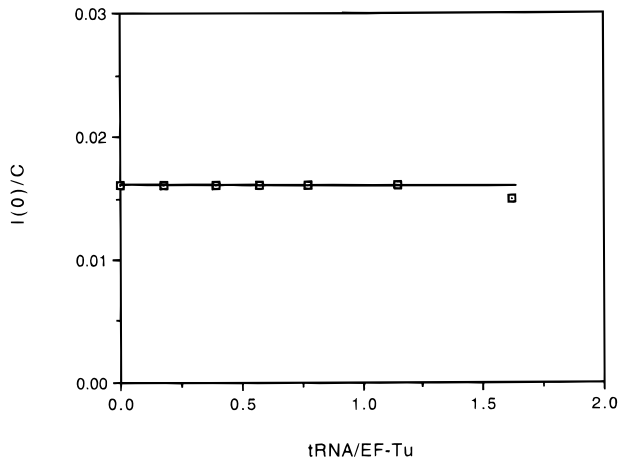

FIGURE 4: $I(0)$ from SANS measurements at constant EF-Tu concentration (120 μM) with varying Phe-tRNA^{Phe} concentrations in polymix buffer containing 70% D_2O at 37 °C. In this buffer the tRNA contrast is negligible and the $I(0)$ essentially corresponds to the protein scattering only.

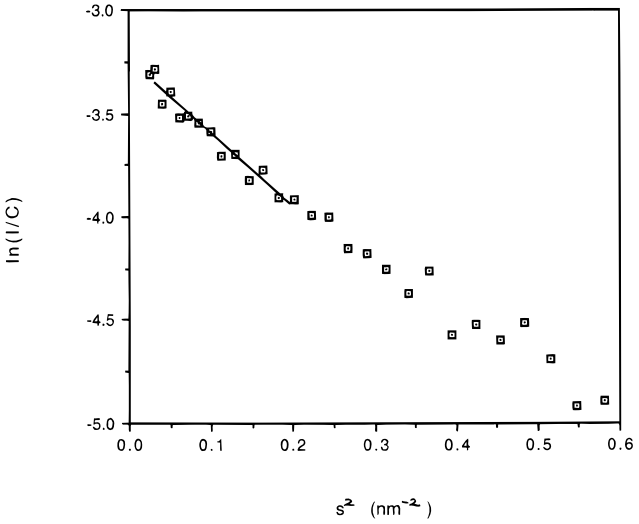

FIGURE 5: Guinier plot of the SANS measurement of the yeast/*T. aquaticus* Phe-tRNA·EF-Tu·GDPNP ternary complex in solvent conditions similar to the mother liquor of crystal growth. Complex concentration was 1.8 mg/mL. The fit is for $0.6 < sR_g < 1.4$.

squares in Figure 3B are for increasing EF-Tu concentrations in the presence of nonacylated tRNA^{Phe}. The calculated line through these points, parallel to the line for free EF-Tu, shows that there is no complex formation under these conditions. The dissociation constant for the binding of EF-Tu·GTP and deacylated tRNA^{Phe} must therefore be considerably larger than 10^{-4} M.

The $I(0)$ values corresponding to titrations of Phe-tRNA^{Phe} (maintained at a constant concentration of 100 μM) by EF-Tu·GTP from 0 to 330 μM, at 6 and 37 °C, are also shown in Figure 3, panels A and B, respectively. At both temperatures $I(0)$ increases steeply upon addition of EF-Tu up to about 100 μM. Beyond this point both curves continue to increase with a smaller slope corresponding to free EF-Tu. The intercepts at the ordinate give the $I(0)$ value of free aminoacyl-tRNA, from which the correct molar mass of about 25 000 g/mol was estimated (*23*, *42*). The steep, initial slopes of the data points fit with the lines calculated for increasing concentrations of 1:1 ternary complex with no free protein [the ratio of $I(0)$ for 1:1 complex to $I(0)$ for free

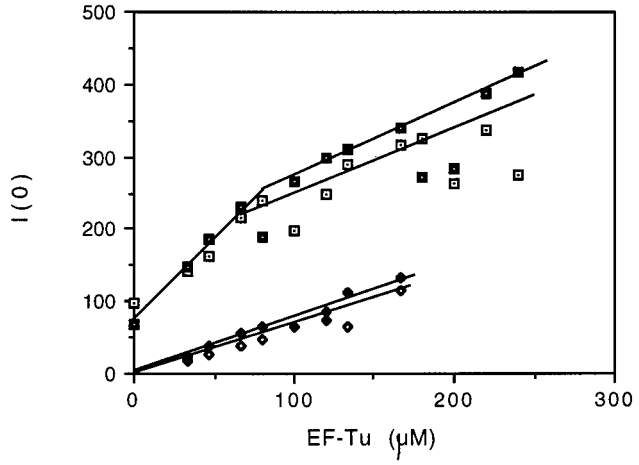

FIGURE 6: SAXS measurements at constant Phe-tRNA^{Phe} with varying EF-Tu concentrations at 5 °C (closed symbols) and at 37 °C (open symbols). $I(0)$ is plotted as a function of EF-Tu in the absence (◇, ◆) and presence (⊡, ◘) of 100 μM Phe-tRNA^{Phe}.

Phe-tRNA^{Phe} was calculated from their neutron scattering amplitudes to be 5.7]. PAGE analysis of these samples also confirmed that there was no free EF-Tu·GTP in this region of the titrations (see Figure 2A). From the $I(0)$ values for free EF-Tu and aminoacyl-tRNA and their dependence on the relative concentrations in the mixture, it was concluded, therefore, that the ternary complex between EF-Tu·GTP and aminoacyl-tRNA has 1:1 stoichiometry at both temperatures.

In the titrations shown in Figure 3, the slopes of $I(0)$ and the ratios of $I(0)$ at 100 μM EF-Tu to $I(0)$ for free tRNA correspond, within the errors, to that expected for a 1:1 stoichiometry between Phe-tRNA^{Phe} and EF-Tu·GTP. The absolute $I(0)$ values at 100 μM EF-Tu, however, are lower than the calculated ones for the 1:1 complex. This may also be due to a systematic overestimate of the EF-Tu concentration and interparticle effects due to the charge on the complex. It should be noted that, because of the errors, the data points could be fitted equally well with a breakpoint at an apparent EF-Tu concentration between 100 and 140 μM. This uncertainty does not weaken the conclusion concerning the 1:1 complex.

The hypothesis of the extended ternary complex (*5*) predicted that titration with an aminoacyl-tRNA from zero to high concentrations in the presence of EF-Tu·GTP should lead to the formation of a complex between 2 molecules of EF-Tu and 1 aminoacyl-tRNA. The most sensitive neutron scattering assay to test this hypothesis is to use a buffer containing 70% D_2O. Under such conditions, tRNA is contrast-matched and its scattering at small angles vanishes (*42*). If extended ternary complex were formed, one would expect a 2-fold increase in $I(0)$ as aminoacyl-tRNA is titrated from zero concentration to excess over EF-Tu. The cause of such an increase in $I(0)$ would be the putative pairing of 2 EF-Tu molecules bound to 1 aminoacyl-tRNA molecule at a molar ratio tRNA:EF-Tu close to 0.5. For a ternary complex with the classical 1:1 stoichiometry between EF-Tu and aminoacyl-tRNA, the scattering intensity $I(0)$ would remain constant. The $I(0)$ values measured in 70% D_2O buffer, as the concentration of aminoacyl-tRNA increased for a molar ratio with EF-Tu from 0 to 1.7 is plotted in Figure 4. They are virtually constant with Phe-tRNA^{Phe} concentration, showing that any complex formed in this range contains only one EF-Tu molecule.

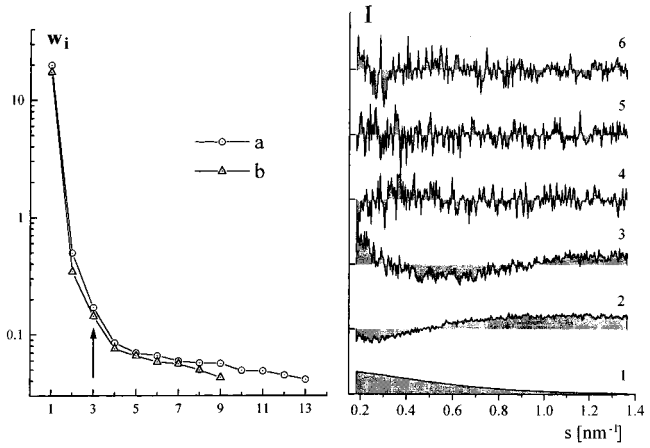

FIGURE 7: Singular value decomposition of the X-ray titration experiments. Left panel: Logarithm of the magnitude of the singular values (w_i) of the scattering intensity matrix ***D*** in the titration experiments at 5 °C (trace a) and 37 °C (trace b) is plotted against their ordinal values. The vertical arrow indicates the number of linearly independent scattering components. Right panel: Intensity on an arbitrary scale of the first six singular vectors arranged in descending order of their singular values. Vectors 1−3 correspond to the scattering from the components, whereas vectors 4−6 represent mainly noise.

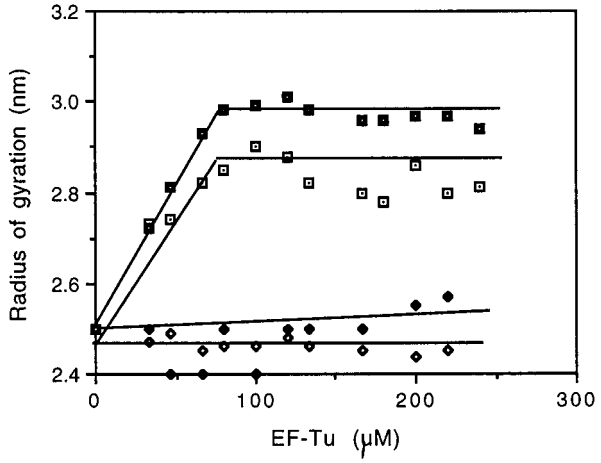

FIGURE 8: Change in R_g as the complex is formed between EF-Tu·GTP and Phe-tRNA^{Phe}. SAXS measurements were performed at 37 °C (open symbols) and at 5 °C (closed symbols) at varying EF-Tu concentrations in the presence (⊡, ◘) and absence (◇, ◆) of 100 μM Phe-tRNA^{Phe}.

Table 1: Structural Parameters of EF-Tu, tRNA, and the Complex in Solution

sample	R_g exp, nm	R_g calc (nm)	$\Delta\rho$ (e/nm^3)	χ
EF-Tu	2.48 ± 0.03	2.36	80	1.04
tRNA	2.28 ± 0.02	2.26	30	0.86
complex	2.96 ± 0.03	3.04	80/30	0.76

(B) Yeast/T. aquaticus Hybrid Complex. SANS data on the yeast/*T. aquaticus* Phe-tRNA·EF-Tu·GDPNP complex at 1.8 mg/mL were collected at 5 °C. In these conditions, interparticle effects are negliglible. The Guinier plot, shown in Figure 5, yields an R_g of 3.3 (± 0.1) nm using the $0.6 < sR_g < 1.4$ range, which is in good agreement with the R_g calculated from the crystal structure (*14*) and with the R_g determined from the *E. coli* Phe-tRNA^{Phe}·EF-Tu·GTP ternary complex in polymix buffer. On an absolute scale, the value of the forward scattered intensity was in full agreement with the scattering mass of the 1:1 EF-Tu·tRNA complex.

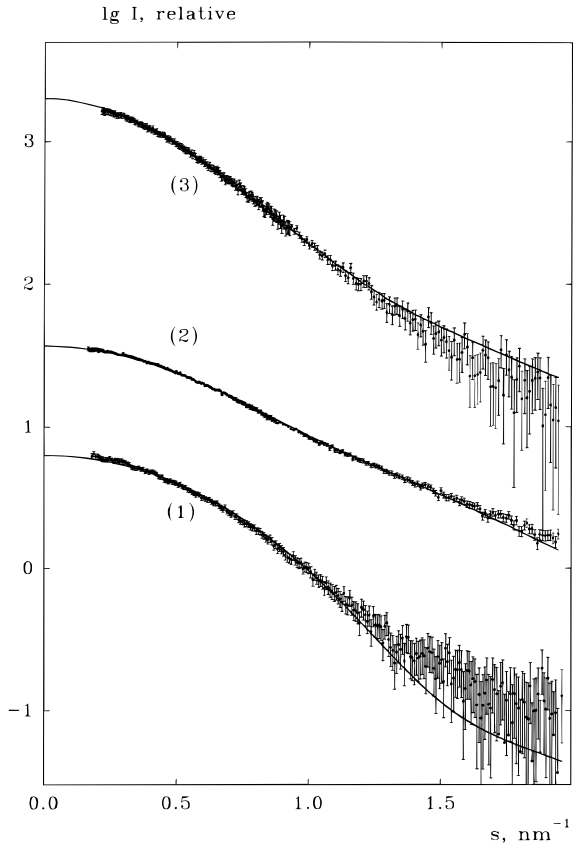

FIGURE 9: Comparisons of the experimental SAXS scattering patterns with those calculated from crystal structures. Experimental data for EF-Tu·GTP (1), Phe-tRNA^{Phe} (2), and their complex (3) at 5 °C are plotted as dots with error bars. Calculated curves are drawn in full lines, respectively, for EF-Tu·GTP from *T. aquaticus* (*32*), for tRNA^{Phe} from *S. cerevisiae* (*33*) and for the ternary complex between EF-Tu from *T. aquaticus*, Phe-tRNA^{Phe} from *S. cerevisiae*, and GDPNP (*14*).

Furthermore, these results show no evidence of trimeric assemblies in the solution, as was previously suggested to be involved in the growth of the Phe-tRNA·EF-Tu·GDPNP crystals (*14*). It may be recalled that the solvent used in these experiments was very close in composition to the mother liquor in the crystals.

Small-Angle X-ray Scattering. Titrations, similar to those performed for neutron scattering, were also analyzed by small-angle solution X-ray scattering (SAXS) at 5 and at 37 °C. Here, shorter measurement times allowed an analysis of full titrations of EF-Tu, aminoacyl-tRNA, and ternary complex at both low and high temperatures (Figure 6).

The molecular masses calculated from the forward scattering by reference to a solution of 10 mg/mL bovine serum albumin (BSA) were 25 ± 3 kDa for tRNA, 45 ± 5 kDa for EF-Tu, and 67 ± 5 kDa for the ternary complex. As a further check of consistency, the complete data set corresponding to the titrations was analyzed by singular value decomposition (Materials and Methods). This analysis (Figure 7) indicates that the system can be fully described with three components corresponding to tRNA, EF-Tu, and ternary complex and excludes the presence of significant amounts of other complexes. This conclusion is also corroborated by the close correspondence between scattering patterns obtained from tRNA or EF-Tu alone and those obtained from component analysis of the composite mixtures.

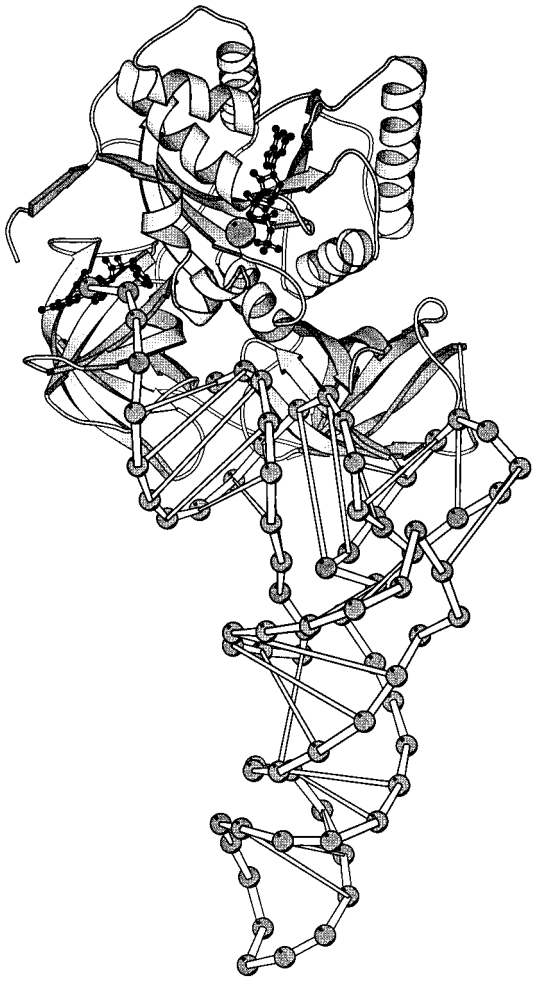

FIGURE 10: Ternary complex crystal structure of yeast Phe-tRNA^{Phe} and *T. aquaticus* EF-Tu·GDPNP (PDB entry code 1TTT). EF-Tu is shown as a structural cartoon and Phe-tRNA as a P-trace with thin bars representing base pairs. The aminoacyl group and the GDPNP cofactor are indicated in ball-and-stick representation, and the Mg^{2+} ion bound together with the cofactor is indicated by the ionic sphere. The figure was produced with Molscript (*46*).

The results confirm that there is a 1:1 stoichiometry between EF-Tu and Phe-tRNA^{Phe}, as determined both from molecular weight estimates and from the breakpoints in the titration curves (Figure 6). There is a small, but significant, increase in R_g when the temperature is switched from 37 to 5 °C (Figure 8).

The high brilliance of synchrotron radiation allows a more detailed study of the scattering patterns. Although solution X-ray scattering cannot be used to determine the three-dimensional structure of a macromolecule at high resolution, the method is ideally suited to test models obtained from, e.g., crystal structures. In Figure 9, the experimental scattering intensities from the EF-Tu·GTP·Phe-tRNA^{Phe} complex as well as from free EF-Tu·GTP and free Phe-tRNA^{Phe} are compared with those calculated from their respective crystal structures (*14*, *32*, *33*). The structural parameters are summarized in Table 1.

The scattering curve from the complex can be well fitted using the scattering amplitudes of its components, each with its contrast in the solvation shell as required for the best CRYSOL fits. This demonstrates that the crystal structure of the ternary complex obtained with *T. aquaticus* EF-Tu, Phe tRNA^{Phe} from yeast, and a GTP analogue (*14*, Figure

10) is practically identical with the solution structure of the ternary complex obtained under optimal buffer conditions (*15*) with native GTP and with both EF-Tu and Phe-tRNA^{Phe} from *E. coli*.

The scattering data from the Phe-tRNA^{Phe} are also neatly fitted by the calculated curve and the contrast in the solvation shell corresponds to a density of 1.09 g/cm^3 in this shell (the electron density of water is 334 e/nm^3), which correlates well with the results obtained earlier for a number of macromolecules (*34*, *43*). This suggests that the crystal and solution structures of the tRNA are the same.

For EF-Tu·GTP, a very high contrast in the solvation shell (corresponding to a density of 1.24 g/cm^3) was required to fit the data, and the fit was still not as good as for tRNA. Comparison of the profiles of the calculated and experimental curves indicate that the particle in the crystal is more compact than in solution. This suggests that EF-Tu·GTP in solution adopts a more open conformation and that its interaction with aminoacyl-tRNA stabilizes a more compact conformation common to both the solution and the crystal.

DISCUSSION

The physicochemical measurements presented above clearly indicate that EF-Tu·GTP indeed forms a 1:1 complex with aminoacyl-tRNA. They also demonstrate that the crystal structure, obtained with Phe-tRNA^{Phe} from yeast, a thermophile EF-Tu, and a GTP analogue instead of GTP (*14*), is remarkably close to the solution structure of the ternary complex obtained with *E. coli* components and native GTP (see Figure 9). Furthermore, the suggestion that the trimeric assembly observed in the asymmetric unit of the crystal structure could be a physiological form of the ternary complex (*14*) can now be rejected, since trimers were not observed at conditions closely resembling the mother liquor of the crystal growth (Figure 5).

The primary aim of the present study was to critically examine the putative existence of an extended ternary complex, consisting of 2 EF-Tu·GTPs and 1 aminoacyl-tRNA (*5*). This hypothesis was based on biochemical evidence obtained in deacylation protection assays (*5*, *6*). It was used to rationalize the parallel, independent observations that there seem to be 2 GTPs hydrolyzed on EF-Tu/peptide bond in poly(U) translation (*3*, *5*, *10*, *44*). The present neutron and X-ray scattering experiments give direct information about the molecular weight of the ternary complex and are therefore more powerful for stoichiometry estimates than previous techniques that only rely on careful titrations but do not provide structural information. The present data were obtained under buffer conditions identical with those where a 2:1 stoichiometry of GTP hydrolysis on EF-Tu/peptide bond was observed (*3*, *5*). Given the present evidence, it is concluded that the earlier hypothesis that aminoacyl-tRNA enters the ribosome in an extended ternary complex should be discarded.

The present experiments were done at both 5 and 37 °C and cover a broad range of concentrations of both EF-Tu and aminoacyl-tRNA. Despite this, there is no tendency for 1 tRNA to bind 2 molecules of EF-Tu, even when EF-Tu is in large excess or when the temperature is shifted from low to high values. This also rules out another suggestion, based on gel-filtration experiments (*12*), that an extended ternary complex forms when EF-Tu is in excess over aminoacyl-tRNA but otherwise not. The data also contradict a previous model suggesting that stoichiometry depends on temperature (*13*). There is presently no clear explanation why the interpretations of these biochemical results are in such direct disagreement with the findings presented here. One possibility is that the small but significant change in the radius of gyration of the ternary complex by temperature as observed here (see Figures 3 and 6) reflects a subtle structural change that may account for a temperature dependence of the RNase A protection pattern.

With the extended ternary complex ruled out, a new explanation must be sought for how 2 GTPs are hydrolyzed on EF-Tu for every peptide bond (*5*, *10*) or conditionally depending on the mRNA context (*12*). A plausible mechanism would involve a handshaking between two EF-Tus on the ribosome, and this raises intriguing questions concerning how 2 EF-Tus or 2 ternary complexes may interact. Indirect support for such interactions between EF-Tu molecules comes from in vivo observations of synergistic interactions between EF-Tus from mutated genes (*45*). However, it may also be necessary at this point to critically reinspect these previous observations, to establish if they hide an artifact despite the impressive number of reports that support the notion of 2 GTPs hydrolyzed/peptide bond in EF-Tu function (*3*, *5*, *10*−*12*, *44*).

REFERENCES

1. Kaziro, Y. (1978) *Biochim. Biophys. Acta 505*, 95−127.
2. Thompson, R. C., Dix, D. B., and Eccleston, J. F. (1980) *J. Biol. Chem 255*, 11088−11090.
3. Bilgin. N., Claesens, F., Pahverk, H., and Ehrenberg, M. (1992) *J. Mol. Biol. 224*, 1011−1027.
4. Ruusala, T., Ehrenberg, M., and Kurland, C. G. (1982) *EMBO J. 1*, 75−78.
5. Ehrenberg, M., Rojas, A.-M., Weiser, J., and Kurland, C. G. (1990) *J. Mol. Biol. 211*, 739−749.
6. Tapio, S., Bilgin, N., and Ehrenberg, M. (1990) *Eur. J. Biochem. 188*, 347.
7. Antonsson, B., Leberman, R., Jacrot, B., and Zaccai, G. (1986) *Biochemistry 25*, 3655−3659.
8. Ebel, C., Gunet, F., Langowski, J., Urbanke, C., Gagnon J., and Zaccai, G. (1992) *J. Mol. Biol. 223*, 361−371.
9. Bensch, K., Pieper, U., Ott, G., Schirmer, N., Sprinzl, M., and Pingoud, A. (1991) *Biochimie 73*, 1045−1050.
10. Weijland, A., and Parmeggiani, A. (1993) *Science 259*, 1311.
11. Weijland, A., Parlato, G., and Parmeggiani, A. (1994) *Biochemistry 33*, 10711−10717.
12. Rodnina, M. V., and Wintermeyer, W. (1995) *Proc. Natl. Acad. Sci. U.S.A. 92*, 1945−1949.
13. Bilgin, N., and Ehrenberg, M. (1995) *Biochemistry 34*, 715−719.
14. Nissen, P., Kjeldgaard, M., Thirup, S., Polekhina, G., Reshetnikova, L., Clark, B. F. C., and Nyborg, J. (1995) *Science 270*, 1464−1472.
15. Ehrenberg, M., Bilgin, N., and Kurland, C. G. (1990) in *Ribosomes and Protein Synthesis: A Practical Approach* (Spedding, G., Ed.) pp 101−129, IRL Press, Oxford, England.
16. Jelenc, P., and Kurland, C. G. (1979) *Proc. Natl. Acad. Sci. U.S.A. 76*, 3174−3178.
17. Bradford, M. M. (1976) *Anal. Biochem. 72*, 248−254.
18. Gillam, J. C., Millward, S., Ble, D., Von Tigerstrom, M., Wiemmer, E., and Tener, G. M. (1967) *Biochemistry 6*, 3043−3056.
19. Holmes, N. M., Hurd, R. E., Reid, B. R., Rimmerman, R. A., and Hatfield, G. W. (1975) *Proc. Natl. Acad. Sci U.S.A. 72*, 1068−1071.

20. Nissen, P., Reshetnikova, L., Siboska, G., Polekhina, G., Thirup, S., Kjeldgaard, M., Clark, B. F. C., and Nyborg, J. (1994) *FEBS Lett. 356*, 165−168.
21. Ibel, K. (1976) *J. Appl. Crystallogr. 9*, 630−643.
22. Lindner P., May R. P., and Timmins, P. A. (1992) Upgrading of the SANS instrument D11 at the ILL, *Physica B 180−181*, 967−972.
23. Jacrot, B., and Zaccai, G. (1981) *Biopolymers 20*, 2414−2426.
24. Guinier, A., and Fournet G. (1955) in *Small Angle Scattering of X-rays*, Wiley, New York.
25. Zaccai, G., and Jacrot, B. (1983) *Annu. Rev. Biophys. Bioeng. 12*, 139−157.
26. Koch, M. H. J., and Bordas, J. (1983) *Nucl. Instrum. Methods 208*, 461−469.
27. Boulin, C., Kempf, R., Koch, M. H. J., and Mc Laughlin, S. M. (1986) *Nucl. Instrum. Methods A249*, 399−407.
28. Boulin, C. J., Kempf, R., Gabriel, A., and Koch, M. H. J. (1988) *Nucl. Instrum. Methods A269*, 312−320.
29. Gabriel, A., and Dauvergne, F. (1982) *Nucl. Instrum. Methods 208*, 223.
30. Svergun, D. I., Semenyuk, A. V., and Feigin, L. A. (1988) *Acta Crystallogr. A44*, 244−250.
31. Svergun, D. I. (1992) *J. Appl. Crystallogr. 25*, 495−503.
32. Kjeldgaard, M., Nissen, P., Thirup, S., and Nyborg, J. (1993) *Structure 1*, 35−50.
33. Westhof, E., Dumas, P., and Moras, D. (1988) *Acta Crystallogr. A44*, 112−123.
34. Svergun, D. I., Barberato, C., and Koch, M. H. J. (1995) *J. Appl. Crystallogr. 28*, 768−773.
35. Svergun, D. I. (1991) *J. Appl. Crystallogr. 24*, 485−492.
36. Svergun, D. I. (1994) *Acta Crystallogr. A50*, 391−402.
37. Malinowski, E. R., and Howery, D. G. (1980) in *Factor Analysis in Chemistry*, Wiley, New York.
38. Guller, S. R., Gilette, P. C., Ishida, H., and Koenig, J. L. (1984) *Appl. Spectrosc. 38*, 495−500.
39. Rossi, T. M., and Warner, I. M. (1986) *Anal. Chem. 58*, 810−815.
40. Schmetterer, L. (1966) in *Einfuhrung in die mathematische Statistik*, Springer-Verlag, New York.
41. Lawson, C. L., and Hanson, R. J. (1974) in *Solving Least Squares Problems*, Prentice Hall, Englewood Cliffs, NJ.
42. Dessen, P., Blanquet, S., Zaccai, G., and Jacrot, B. (1978) *J. Mol. Biol. 126*, 293−313.
43. Svergun, D. I., Barberato, C., Koch, M. H. J., Fettler, L., and Vachette, P. (1997) *Proteins: Struct., Funct., Genet. 27*, 110−117.
44. Scoble, J., Bilgin, N., and Ehrenberg, M. (1994) *Biochimie 76*, 59−62.
45. Vijgenboom, E., Vink, T., Kraal, B., and Bosch, L. (1985) *EMBO J. 4*, 1049−1052.
46. Kraulis, P. J. (1991) *J. Appl. Crystallogr. 24*, 946−950.

BI9802869